Axial-azimuthal hybrid-direct kinetic simulation of Hall effect thrusters

IEPC-2015-286／ISTS-2015-b-286

Presented at Joint Conference of 30th International Symposium on Space Technology and Science, 34th International Electric Propulsion Conference and 6th Nano-satellite Symposium
Hyogo-Kobe, Japan
July 4–10, 2015

Kentaro Hara* and Iain D. Boyd†
University of Michigan, Ann Arbor, MI, 48105, USA

A two-dimensional hybrid-direct kinetic (DK) simulation is presented to investigate low-frequency plasma oscillations in the axial and azimuthal directions of a Hall effect thruster. A DK method, in which the kinetic equations are solved directly on discrete phase space, is used for ions while a fluid model is used for electrons. Verification of the DK method is performed under a static electric field and the swirling effect of ions is captured due to the ion magnetization. In comparison to one-dimensional hybrid-DK simulations [Hara et al. J. Appl. Phys. 115, 203304 (2014)], mode transition of the discharge plasma oscillations is studied using the two-dimensional hybrid-DK simulation. At a small magnetic field strength, the discharge plasma oscillation in the axial direction dominates. At a larger magnetic field strength, stabilization of the discharge current oscillation is observed. Although the axial oscillations are not completely stabilized, normalized surface plots of the axially-integrated ion number density show indication of azimuthally rotating spokes.

I. Introduction

Several experiments have observed low-frequency rotating spokes in Hall effect thrusters (HETs). Parker *et al.*[1] showed the correlation between plasma density, light emission, and electron currents, using high-speed cameras and Langmuir probes. It was also observed that the spoke rotates in the $E \times B$ direction with a speed of 1200− 2800 m/s, which is significantly smaller than the $E \times B$ drift. Ellison[2] measured the electron current induced by rotating spokes using a segmented anode in cylindrical Hall thrusters. It was concluded that over half of the total current is conducted by the spoke. Through the use of high-speed Langmuir probe systems[3] and high-speed cameras,[4] azimuthally rotating spokes have been investigated by Sekerak at the University of Michigan.[5] It is shown in Ref. 5 that the emitted light intensity oscillates coherently in the azimuthal direction. In addition, $m = 1$ spoke modes are observed in cylindrical HETs whereas $m > 2$ are observed in the H6 annular thruster.

A radial-axial hybrid-PIC model has been used the most widely in the HET community. A 2D PIC method is used for ions and neutral atoms and a quasi-1D continuum approach is used for electrons. HPHall, originally developed by Fife and Martinez-Sanchez,[6] has been further extended by several researchers, including Parra *et al.*,[7] Cheng,[8] and Hofer *et al.*[9] Koo and Boyd[10] developed a similar 2D model in order to investigate the effects of anomalous electron transport on the discharge plasma. A 2D hybrid-PIC simulation, based on the 1D hybrid-DK type simulation by Boeuf and Garrigues,[11] was further developed by Hagelaar *et al.*,[12] which uses a similar formulation as HPHall.

Although the hybrid-PIC methods employ a quasi-1D approach for electrons, full-2D models have been developed. Keidar *et al.*[13] developed a 2D continuum simulation with a detailed plasma-wall interaction model. Mikellides *et al.*[14] have developed a 2D continuum model, called Hall2De. A magnetic field aligned mesh is used and the domain can be extended into the far-field plume because of the reduced computation

*Postdoctoral Research Fellow, Department of Aerospace Engineering, University of Michigan, kenhara@umich.edu
†Professor, Department of Aerospace Engineering, University of Michigan, iainboyd@umich.edu

cost compared to particle methods. Geng *et al.*[15] revisited the thermalized potential assumption used in the state-of-the-art hybrid-PIC simulations, in which they suggested that a full 2D potential solver is required.

2D full-PIC methods have also been used to model small-scale turbulence effects and plasma-wall interactions. One of the first developments was by Hirakawa and Arakawa.[16] Szabo[17] developed a fully-PIC/DSMC simulation in the radial-axial directions. Cho[18] also presented a similar full-PIC method analyzing the effects of artificial mobility and permittivity. A 2D axial-azimuthal simulation by Adam *et al.*[19] showed that a high frequency turbulence type oscillation exists at the exhaust of the thruster. A similar numerical simulation was recently presented by Coche and Garrigues.[20]

In this paper, a 2D hybrid-DK simulation is constructed. A 2D axial-azimuthal hybrid-PIC simulation was recently presented by Lam *et al.*,[21] but it was shown that there were numerical instabilities that made the solver stop at 0.1 μs, which is too short to discuss any low-frequency oscillations. A 2D continuum model was used for the electrons in their model. One advantage of using DK simulation is that the statical noise in PIC is eliminated, so the hybrid-DK simulation may generate numerically quiet results.

II. Hypotheses for Low-Frequency Spokes

Sekerak made two hypotheses about the low-frequency rotating spokes in Ref. 5. It was indicated that the rotating spokes are an oscillation wave that results from (1) stabilization of the ionization front and (2) interaction with the outer channel wall.

The first hypothesis is supported by the observation that local ionization oscillations in the azimuthal direction disappear when global ionization mode, *i.e.* breathing mode, occurs. The second is supported by another observation in magnetically shielded Hall thrusters, where azimuthal spokes are not seen despite the stronger magnetic field strengths compared to conventional thrusters. It was shown that the only occasion for the spokes to appear is when the magnetic shielding is imperfect and the hot plasma touches the *outer* wall at high magnetic field strengths. In addition, several dispersion relation analyses were performed in Ref. 5, but all the high-frequency oscillations related to electron transport disagree with the spoke characteristics. The low-frequency oscillations suggests that the oscillation frequency is heavily dependent on the slow neutral atom flow.

A hypothesis that can be answered using the 2D hybrid kinetic-continuum model is whether an azimuthally rotating spoke is generated by a local ionization oscillation event. As shown in Fig. 1, the ions move axially and electrons move azimuthally. The observed spoke velocity in Ref. 5 was $1500 - 2200$ m/s

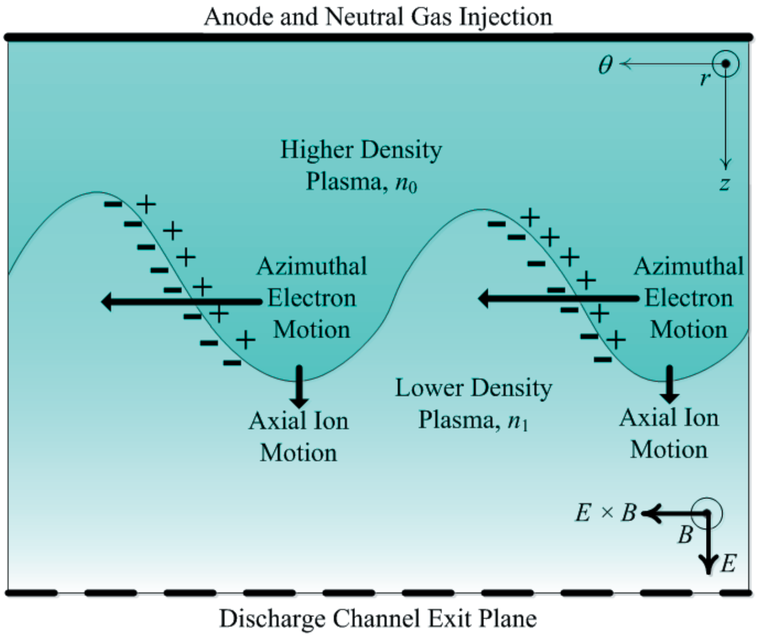

Figure 1. Possible mechanism of the rotating spokes. Diagram of $z - \theta$ plasma of discharge channel shown exaggerated ionization front. Reproduced from Fig. 5.19 of Ref. 5.

in the azimuthal direction whereas the $E \times B$ drift of electrons is on the order of 10^6 m/s at maximum. Sekerak[5] proposed a simple mechanism of the azimuthally rotating spokes as an ambipolar diffusion from the energy balance. Ambipolar diffusion sets an electric field that accelerates ions to the Bohm velocity, which is the ion acoustic speed. In this case, it can be assumed that the electron energy is dominated by the $E \times B$ drift, so

$$v_\theta = \sqrt{\frac{\frac{1}{2} m_e v_{E\times B}^2}{m_i}} \approx \sqrt{\frac{m_e}{m_i}} v_{E\times B}$$

A similar mechanism was also suggested by Boeuf.[22] The spoke velocity is explained as a *critical ionization velocity*. Ions gain energy across the moving sheath that is on the order of the ionization potential for xenon atoms. $v_\theta = (2e\Delta\phi/m_i)^{1/2}$, where $\Delta\phi$ is the ionization potential, *e.g.* $\Delta\phi \approx 12.1$ eV for xenon atoms.

Note that the spoke velocity is not equal to the ion mean velocity in the azimuthal direction. This is supported by an experimental observation in Ref. 23. It was indicated that the ion swirl velocity, *i.e.* the ion mean velocity in the azimuthal direction, is approximately 250 m/s, which is much smaller than the rotating spoke velocity obtained from experiments. In addition, in this situation, the spoke velocity must be a strong function of magnetic field strength, but Sekerak's experiment showed that spoke velocity and magnetic field strengths are uncorrelated.

Finally, the use of a 2D axial-azimuthal simulation is justified by the observations that spokes fill the channel radially from the inner wall to the outer. Thus, the plasma structure can essentially be averaged in the radial direction. The experiments in Ref. 5 showed that the azimuthal spokes have wave numbers in the range of $k_\theta = 30 - 80$ rad/m. It was stated by Sekerak[5] that "*What is needed is a $z - \theta$ simulation, either kinetic, fluid, PIC or a hybrid of any of these, that can resolve time steps of 1 µs or less (in order to resolve 10's kHz oscillation) and wave numbers less than 100 rad/m. The domain should be from the anode out at least one channel width downstream of the exit plane for a time duration of several hundred micro-seconds. Finally, in the limit of 1D in the z-direction, it should recover the 10-30 kHz axial breathing mode.*" The purpose of the present 2D hybrid-DK simulation is to fulfill these criteria and observe low-frequency, low wavenumber oscillations.

III. 2D Kinetic Model

The axial-azimuthal domain in cylindrical coordinates is approximated as a 2D planar domain. This significantly reduces the computational cost, as the third dimension in velocity space (here, the radial direction) can be neglected. If the total number of discretized phase space elements for a 2D2V simulation is N_{4V}, then it is $N_{4V} N_V$ for a 2D3V simulation, where N_V is the number of velocity bins in the extra dimension. Thus, the computational cost increases by at least a factor of N_V when adding another dimension.

A. 2D Axial-Azimuthal Kinetic Simulation

A schematic diagram of the 2D axial-azimuthal simulation is shown in Fig. 2. Figure 2(a) shows the cylindrical coordinates in a Hall thruster discharge channel. The radial direction pointing outwards follows the magnetic field orientation. In the 2D domain, shown in Fig. 2(b), the axial and azimuthal coordinates correspond to the x and y directions, respectively. Therefore, the $E_x \times B_r$ drift is in the y direction, $v_x B_r$ is in the y direction, and $v_y B_r$ is in the $-x$ direction.

The 2D kinetic equation can be written as

$$\frac{\partial f}{\partial t} + v_x \frac{\partial f}{\partial x} + v_y \frac{\partial f}{\partial y} + \frac{e}{m_i}(E_x - v_y B_r)\frac{\partial f}{\partial v_x} + \frac{e}{m_i}(E_y + v_x B_r)\frac{\partial f}{\partial v_y} = S. \tag{1}$$

The anode is set at $x = 0$ m and the domain exit is $x = 0.035$ m. The y direction uses a periodic boundary condition. In addition, the Lorentz force can be turned on and off in order to investigate the effect of the gyromotion of ions in the 2D domain. The centrifugal force due to the radial transport is neglected. Equation (1) is based on a magnetic field line pointing outwards of the channel. However, this direction of the magnetic field can also be flipped so that $B_r < 0$.

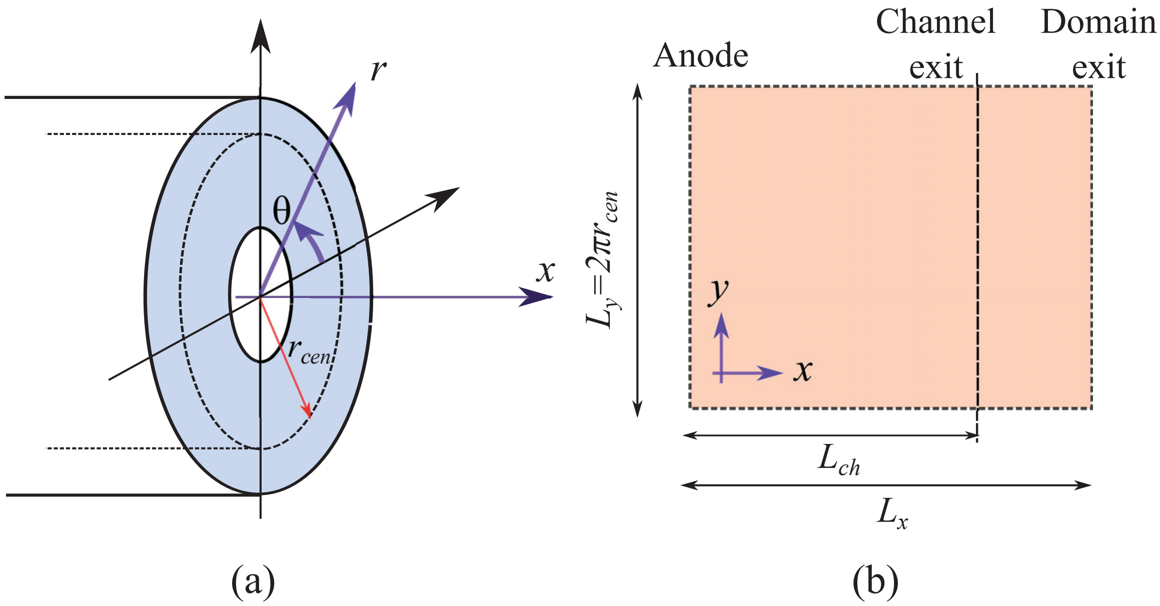

Figure 2. The 2D setup. (a) Cylindrical Coordinates in an annulus, representing a Hall thruster discharge channel. The dashed line in (a) is the plane of interest, expanded into 2D in (b).

B. Discretized 2D DK Model

For the 2D DK model, there are four dimensions, *i.e.* 2D2V. Strang's time splitting becomes more complicated and requires more intermediate time steps for a four dimensional system. The next obvious choice is to split the physical and velocity update, which is similar to a leap-frog scheme in particle methods. This will yield second order accuracy in time integration and would require 2D and 2V updates to be second order accurate. The time integration used is a second-order accurate Runge-Kutta method without any dimensional splitting. Equation (1) without the source term can be written as

$$\frac{\partial f}{\partial t} + L[f(x, y, v_x, v_y)] = 0,$$

where $L[f(x, y, v_x, v_y)]$ consists of the physical and velocity advection terms. Then, a second-order Runge-Kutta method can be written as

$$f^* = f^n + \Delta t L(f^n),$$
$$f^{n+1} = f^n + \frac{\Delta t}{2}\left[L(f^n) + L(f^*)\right].$$

The discretized VDF can be written as $f_{ix,iy,jx,jy}$ where ix, iy, jx, and jy are the cell numbers in the x, y, v_x, and v_y directions, respectively. Then, the discretized flux terms can be written as

$$v_x \frac{\partial f}{\partial x} = \frac{v_x}{\Delta x}(f_{ix+1/2,iy,jx,jy} - f_{ix-1/2,iy,jx,jy}),$$
$$v_y \frac{\partial f}{\partial y} = \frac{v_y}{\Delta y}(f_{ix,iy+1/2,jx,jy} - f_{ix,iy-1/2,jx,jy}),$$
$$a_x \frac{\partial f}{\partial v_x} = \frac{a_x}{\Delta v_x}(f_{ix,iy,jx+1/2,jy} - f_{ix,iy,jx-1/2,jy}),$$
$$a_y \frac{\partial f}{\partial v_y} = \frac{a_y}{\Delta v_y}(f_{ix,iy,jx,jy+1/2} - f_{ix,iy,jx,jy-1/2}),$$

where $a_x = e(E_x - v_y B_r)/m_i$ and $a_y = e(E_y + v_x B_r)/m_i$. The subscripts $+1/2$ and $-1/2$ denote the cell interfaces. For each flux evaluation, the finite volume method with a modified Arora-Roe limiter is used.[24] Note that a_x and a_y are independent of v_x and v_y, respectively.

The time step is restricted by the CFL condition. For the 2D2V DK model using a second-order Runge-Kutta time integration, the time step must follow:

$$\max\left(\frac{v_x\Delta t}{\Delta x}+\frac{v_y\Delta t}{\Delta y}+\frac{a_x\Delta t}{\Delta v_x}+\frac{a_y\Delta t}{\Delta v_y}\right)\leq\alpha, \tag{2}$$

where α is the safety factor. In this model, $\alpha = 0.9$ is used. Equation (2) needs to be satisfied for numerically stable integration. Thus, if the left hand side is above α, the time step is reduced as $\Delta t = \Delta t/N_{CFL}$, where N_{CFL} is the left hand side of Eq. (2) divided by α. For instance, if the left hand side of Eq. (2) is 1.5, $N_{CFL} = 2$ and thus the time step is reduced in half. The collision term is added after the left hand side of Eq. (1) is updated. The domain size and discretization are provided in Table 1.

Table 1. Discretization of 2D DK simulation

Axial domain length	L_x	3.5 cm
Channel length	L_{ch}	2.5 cm
Inner Radius	r_{in}	3.5 cm
Outer Radius	r_{out}	5 cm
Azimuthal length	L_y	$\pi(r_{in}+r_{out}) = 26.7$ cm
Velocity space in axial direction	$[v_{x,min}, v_{x,max}]$	[-15000 m/s, 35000 m/s]
Velocity space in azimuthal direction	$[v_{y,min}, v_{y,max}]$	[-10000 m/s, 10000 m/s]
The number of cells in physical space	$[N_x, N_y]$	[70, 32]
The number of cells in velocity space	$[N_{vx}, N_{vy}]$	[200, 100]
Cell size in physical space	$[\Delta x, \Delta y]$	[0.5 mm, 8.3 mm]
Cell size in velocity space	$[\Delta v_x, \Delta v_y]$	[250 m/s, 200 m/s]

C. 2D Ion Simulation with a Static Electric Field

Here, a static electric field is prescribed and the effect of magnetic fields on the ion acceleration is investigated. For this test case, the source term is neglected: $S = 0$ in Eq. (1).

Electric Field

The prescribed electric field in the x direction is given by.

$$E_x=\frac{7V_d}{L_x}\left(\frac{x}{L_x}\right)^6, \tag{3}$$

and the electric field in the y direction is zero: $E_y = 0$. This corresponds to

$$\phi=V_d\left[1-\left(\frac{x}{L_x}\right)^7\right],$$

where ϕ is the plasma potential. In the simulations, $V_d = 300$ V is assumed. The ions enter the domain at the anode $x = 0$ with a half-Maxwellian. Note that assigning a half-Maxwellian at the ghost cell adjacent to the anode yields a biased-Maxwellian at the anode plane because the probability of particles is shifted with their own velocity. The inlet number density is $n_0 = 10^{15}$ m^{-3} and the ion mean velocity is $u_0 = (\pi k_B T/2m_i)^{1/2}$. For $T = 750$ K and xenon singly charged ions, *i.e.* $m_i = 131$ amu, the ion mean velocity is 273 m/s at the anode.

Magnetic Field

The magnetic field in these simulations is inward pointing, *i.e.* $B_r < 0$. The shape of the magnetic field is the same as the 1D simulations:

$$B_r(x)=B_{max}\exp\left[-\left(\frac{x-L_{ch}}{\Delta L}\right)^2\right]$$

Four different cases are tested: $B_{max} = 0$, 120, 240, and 400 G.

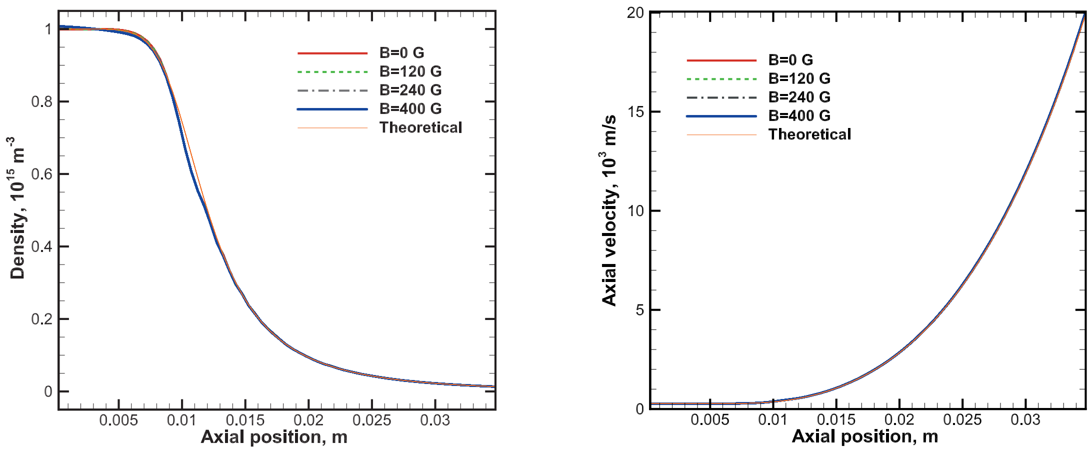

(a) Ion number density

(b) Ion mean velocity in the x direction

Figure 3. Static electric field case using the DK simulation.

Results

Figure 3 shows the steady-state ion number density and mean velocity in the x direction obtained from the DK simulation. Good agreement between the numerical simulations and theory is shown. The effects of the magnetic field on these macroscopic results are small. It can be also seen that there are some discrepancies near $x = 0.01$ m. The relative error can be given by $|\Delta e| = |u_n - u_a|/|u_a|$, where u is the solution and subscripts n and a represent numerical and analytical, respectively. The maximum relative error in $0.007 < x < 0.012$ m can be as large as 8 % for both the ion density and mean velocity. However, it is found that the relative error reduces to within 0.5% in the region of $x > 0.015$ m.

The ion mean velocity in the y direction is shown in Fig. 4. It can be seen that the magnetization yields the ion mean velocity up to 550 m/s at the domain exit. This suggests that a helical structure can be formed for the ion flows in the presence of a radial magnetic field. Such helical structure is reported in Hall thrusters by Sekerak[5] and Smith[25] as well as in a helicon discharge by Siddiqui.[26]

IV. 2D Electron Continuum Model

In order to capture the low-frequency oscillations in the axial and azimuthal directions of the discharge plasma, the present model neglects the effect of radial transport. Hence, a two-dimensional assumption is used.

The electron continuum model is very sensitive to the discharge plasma. The use of a quasineutral assumption is valid for the ion time scales but not for electrons. There are two equations that are not needed to be solved by using the quasineutral assumption: the electron continuity equation and the Poisson equation. Instead, ions and electrons are related to each other through the charge conservation equation assuming only singly-charged ions and electrons.[a] The Poisson equation can no longer be used to calculate the electric field or the plasma potential as the right hand side of the Poisson equation is zero due to the quasineutral assumption. Thus, the electric field needs to be calculated from the charge conservation equation that requires a *linear* dependence of the electron momentum on the electric field. The most common technique in the low-temperature plasma community is to use a drift-diffusion approximation.[b] Once the *nonlinearity*

[a]Charge conservation equation is derived by the ion and electron continuity equations.

[b]Drift-diffusion approximation works if the diffusion effects are dominant in the system and the spatial profile of electron current or flux is smooth.

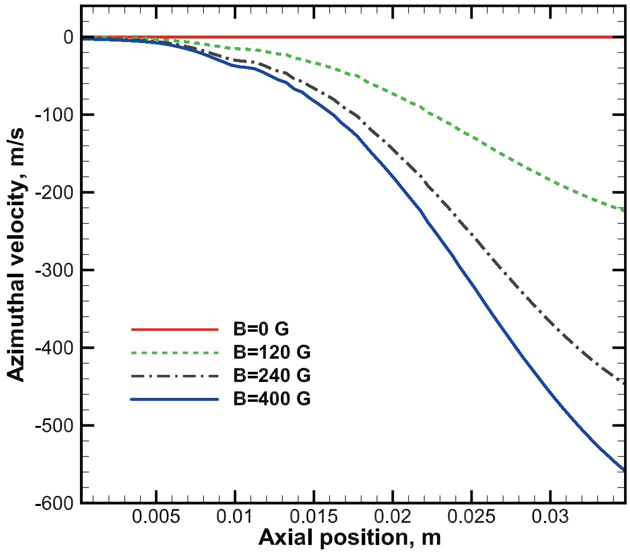

Figure 4. Ion mean velocity in the y direction for the static electric field case using the DK simulation. Note that the azimuthal velocities are negative because the direction of the magnetic field lines is pointing inwards.

of electron momentum, *e.g.* inertia,[c] is introduced, then the charge conservation equation with the nonlinear electron momentum cannot be solved. In this situation, a time-dependent solution to the nonlinear equations may become the only option. However, this will required additional solvers for the electrons as the electron equations and the Poisson equation must be solved without assuming quasineutrality, which is reserved for future work.

A. 2D Charge Conservation Equation

The charge conservation equation can be given by

$$\frac{\partial \sigma}{\partial t} + \nabla \cdot \mathbf{J} = 0, \tag{4}$$

where $\sigma = n_i - n_e$ is the charge and $\mathbf{J} = \mathbf{J}_i - \mathbf{J}_e$ is the total flux. This can be derived from ion and electron mass conservation equations under the assumption that the right hand side is identical, which is only valid when single-charged ions are considered. Using a quasineutral assumption, Eq. (4) can be written as

$$\nabla \cdot \mathbf{J}_e = \nabla \cdot \mathbf{J}_i. \tag{5}$$

B. Electron Momentum

The electron flux is required for the charge conservation equation in Eq. (5) in order to solve for the electric field, or the plasma potential, when using a quasineutral assumption.

The axial momentum equation can be written in a continuum form as

$$mn\left[\frac{\partial u_{ex}}{\partial t} + u_{ex}\frac{\partial u_{ex}}{\partial x} + u_{ey}\frac{\partial u_{ex}}{\partial y}\right] = -\frac{\partial p}{\partial x} - en(E_x - u_{ey}B_r) - mnu_{ex}\nu_m. \tag{6}$$

The drift-diffusion approximation is assumed, so the left hand side of Eq. (6) is zero. For the azimuthal transport, we further assume that $E_y + 1/(en)\partial p/\partial y \approx 0$, which is supported by experimental observations in Ref. 2. The azimuthal momentum equation is written as

$$0 = -eu_{ex}B_r - mu_{ey}\nu_m. \tag{7}$$

[c]The inertial term plays an important role when the electron mean velocity has non-smooth profile, such as discontinuity.

Therefore, the axial and azimuthal electron momentum equations can be written as

$$u_{ex} = -\mu_{\perp}\left(E_x + \frac{1}{en}\frac{\partial p}{\partial x}\right) \tag{8}$$

$$u_{ey} = -\Omega u_{ex} = +\mu_{\perp}\Omega\left(E_x + \frac{1}{en}\frac{\partial p}{\partial x}\right), \tag{9}$$

where $\mu_{\perp} = \mu(1+\Omega^2)^{-1}$ is the cross-field electron mobility, $\mu = e/m\nu_m$ is the electron mobility, and $\Omega = eB_r/m\nu_m$ is the Hall parameter. Note that Eq. (9) reduces to

$$u_{ey} = \frac{1}{B}\left(E_x + \frac{1}{en}\frac{\partial p}{\partial x}\right),$$

for $\Omega \gg 1$. The azimuthal electron mean velocity is the sum of the $E \times B$ drift and the diamagnetic drift, which can be derived from the collisionless guiding center theory. Note that the drift velocities calculated from the guiding center motion are already time-averaged quantities. It is further assumed that the spatial derivative of the electron momentum in the y direction follows

$$\frac{\partial}{\partial y}(nu_{ey}) \simeq \frac{n}{B}\frac{\partial}{\partial y}\left(E_x + \frac{1}{en}\frac{\partial p}{\partial x}\right) \approx 0, \tag{10}$$

so that the electron momentum in the y direction can be neglected in the 2D charge conservation equation.

C. Reviewing the One-Dimensional Case

The 1D charge conservation equation with a quasineutral assumption yields

$$\frac{\partial J_{ex}}{\partial x} = \frac{\partial J_{ix}}{\partial x},$$

where J_{ex} can be given as $J_{ex} = nu_{ex} = -n\mu_{\perp}(E_x + n^{-1}\partial p/\partial x)$ for simplicity. Thus, using $E_x = -\partial\phi/\partial x$, the 1D charge conservation equation can be written as

$$\frac{\partial}{\partial x}\left(n\mu_{\perp}\frac{\partial \phi}{\partial x}\right) = \frac{\partial}{\partial x}\left(\mu_{\perp}\frac{\partial p}{\partial x}\right) + \frac{\partial J_{ix}}{\partial x}, \tag{11}$$

which is now a 2nd-order elliptic PDE that can be solved using linear algebra methods. In discrete form, this equation can be written as

$$\frac{1}{\Delta x}\left(\frac{a_i\phi_{i+1} - b_i\phi_i}{\Delta x} - \frac{b_i\phi_i - c_i\phi_{i-1}}{\Delta x}\right) = S_i,$$

where a_i, b_i, and c_i are the coefficients, ϕ_i is the potential, and S_i is the source term at point i, which is the right hand side of Eq. (11). The coefficients are $a_i = (n\mu_{\perp})_{i+1}$, $b_i = (n\mu_{\perp})_i$, and $c_i = (n\mu_{\perp})_{i-1}$, which are the product of ion number density and the transverse electron mobility. In vector form, this can be written as

$$\mathbf{A}\vec{\phi} = \vec{S}, \tag{12}$$

where $\mathbf{A}$ consists of a_i, b_i, and c_i.

Condition number

The condition number of a matrix defines how well- or ill-conditioned the matrix is. Ill-conditioned matrix means that the matrix is closer to a singular matrix, so it is difficult or impossible to find the solutions. This is characterized by the condition number, typically given as

$$\mathrm{cond}(A) = \frac{\lambda_{\max}}{\lambda_{\min}}, \tag{13}$$

where $\lambda_{\max}$ and $\lambda_{\min}$ are the maximum and minimum eigenvalues of the $\mathbf{A}$ matrix. When the condition number is large, the matrix is more ill-conditioned. In this situation, the matrix should not be solved in the form shown in Eq. (12). For instance, in the Hall thruster discharge plasma, an integration technique is used. The spatially integrated information is used so that the total current and the discharge voltage can be related.

Consider a simple case in which the shape of magnetic field strength and ion density is assumed to follow $\sim \exp\{-[(x - L_{exit})/\Delta L]^2\}$, where $L_{exit} = 0.025$ m and $\Delta L = 0.0125$ m. In calculating the condition number, $B_{max} = 0.018$ T and $n_{i,max} = 10^{18}$ m^{-3} are used. In addition, the momentum transfer collision frequency is assumed to be constant at $\nu_m = 10^7$ s^{-1}. The transverse electron mobility is given by

$$\mu_\perp = \frac{e}{m_e \nu_m}\left[1 + \left(\frac{\omega_B}{\nu_m}\right)^2\right]^{-1},$$

where $\omega_B = eB/m_e$ is the gyrofrequency. Figure 5(a) shows the input conditions to calculate the condition number of the matrix in Eq. (12). It can be seen that the electron mobility can be very small for $\omega_B \gg \nu_m$, which occurs in the regions where the magnetic field strength is at maximum. On the other hand, the electron mobility near the anode can become orders of magnitude larger than that near the channel exit.

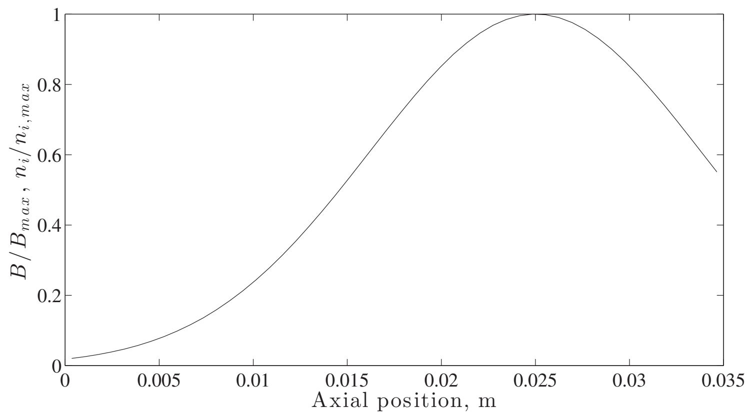

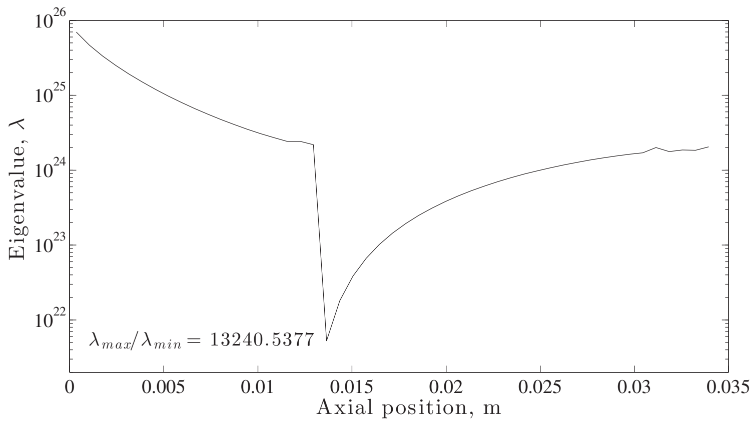

Figure 5. Example of a 1D axial case. (Top) Prescribed magnetic field and assumed ion density. $B_{max} = 0.018$ **T and** $n_{i,max} = 10^{18}$ **m**$^{-3}$ **are assumed. (Bottom) Eigenvalues estimated using the MATLAB EIG function assuming Dirichlet Boundary conditions for potential. The Condition number is 13,240.**

It can be seen from Fig. 5(b) that the condition number is over 10,000, which is very large for a matrix relative to the Poisson or Laplace equation, which is a common elliptic PDE. This means that a small perturbation around the maximum eigenvalue, *e.g.* 10^{-4}, can result in a larger perturbation, *e.g.* $\sim O(1)$ around the minimum eigenvalue. The condition number is calculated using the EIG function in MATLAB. The result suggests that Eq. (12) cannot be converged to obtain a solution unless the right hand side of the equation has small error. The coefficients of matrix $\mathbf{A}$ are orders of magnitude smaller near the channel exit than those near the anode. Therefore, a small change (error) of the potential near the anode can lead to a large change of the potential calculation near the channel exit.

Integration Method

Instead of solving the second-order elliptic PDE, an integration technique can be useful for solving the system. As there are no issues related to condition numbers, the electron momentum equation can be solved with any values of coefficients in Eq. (12). In particular, the quasi-1D approximation in the state-of-the-art computational methods, such as in HPHall and other 2D models, essentially use a similar integration technique. Equation (11) can be integrated once over the axial direction to obtain

$$J_{ix} + J_{ex} = J_d, \tag{14}$$

where J_d is the total flux or the sum of ion and electron fluxes at the anode. Another spatial integration yields

$$V_D = J_d \int \frac{1}{n\mu_\perp} dx - \int \frac{1}{n}\frac{\partial p}{\partial x} dx - \int \frac{J_{ix}}{n\mu_\perp} dx, \tag{15}$$

from which the total flux J_d can be obtained. Then, the electron flux always satisfies the total current conservation in Eq. (14).

The advantage of this method over solving the 2nd order elliptic PDE is that the numerical or physical perturbations in the pressure term can be much smoother because the pressure term is integrated in space and numerical errors can be cancelled out in Eq. (15). On the other hand, the 2nd derivative of pressure exists on the right hand side in Eq. (11). The pressure terms are obtained by forcing the quasineutral condition, which means that the pressure is obtained as a product of ion density and electron temperature. The ion density is updated due to the electric field calculated in the electron fluid model. With a small perturbation in the ion density, the electric field will respond through Eq. (11), which is then fed into the ion transport. Thus, there is no damping mechanism to the pressure perturbation.

New Model

Assuming $J_{ix} \ll J_{iy}$, the ion flux component in the y direction can be neglected. Another assumption is $\partial J_{ey}/\partial y \approx 0$ from Eq. (10). Thus, the charge conservation equation can be given as

$$\frac{\partial}{\partial x}[J_{ix}(x,y) - J_{ex}(x,y)] = 0. \tag{16}$$

One-step integration over the x direction gives

$$J_{ix}(x,y) - J_{ex}(x,y) = J_d(y)$$

Therefore, Eq. (16) can be solved for each y coordinate using an integration technique. The anode current, J_d, is calculated as a function of y and the total anode current can be calculated as

$$J_{tot} = \int J_d(y) dy. \tag{17}$$

D. Electron Energy

The electron energy equation is given by

$$\frac{\partial}{\partial t}(n\varepsilon) + \nabla \cdot [(n\varepsilon + p)\mathbf{u}_e] = \nabla \cdot (\kappa_e \nabla T_e) - en\mathbf{u}_e \cdot \mathbf{E} - S_i - S_w, \tag{18}$$

where κ_e is the heat conductivity, S_i is the electron energy transfer due to inelastic collisions, including electron-impact ionization, stepwise ionization, and excitation, and S_w is the wall collision term, given by

$$\kappa_e = 2.4 \cdot nT_{eV}k_B \frac{\mu}{1+\Omega^2}$$

$$S_i = \sum_j n\nu_j \Delta\epsilon_j$$

$$S_w = n\nu_w \Delta\epsilon_w.$$

Note that elastic collision transfer is assumed to be negligible. The total energy is given as the sum of the electron thermal energy, *i.e.* the electron temperature, and the kinetic energy

$$\varepsilon = \frac{3}{2} T_{eV} + K_{eV},$$

where K_{eV} is the kinetic energy. Here, one approximation is employed. The electron pressure gradient and the electric field in the azimuthal direction are neglected in the momentum equation. As the electron velocity in the azimuthal direction is much larger than that in the axial direction, even a small electric field in the azimuthal direction can lead to a significant heat source.[d] Therefore,

$$\frac{\partial}{\partial t}(n\varepsilon) + \nabla \cdot (n\varepsilon \mathbf{u}_e) + \frac{\partial p u_{ex}}{\partial x} = \nabla \cdot \left(\kappa_e \nabla \frac{2}{3}\varepsilon\right) - enu_{ex}E_x - S_i - S_w \tag{19}$$

is solved. Note that the thermal conductivity term is assumed to follow the effective electron temperature including the effect of kinetic energy instead of the actual electron temperature. The right hand side is explicitly obtained using the variables at the current time step. In the present model, the conductive flux and the convective heat flux are assumed to be implicit and the other terms are explicit in time. In addition, the convective heat flux employs first-order upwind discretization.

In the 2D simulation, hypre, a linear algebra library developed at LLNL, is used to solve for the system of equations. The Generalized Minimal Residual (GMRES) method with a multigrid preconditioner is used for convergence. Tolerance is set to 10^{-14} and the maximum number of iteration is 50. However, convergence for the time-implicit electron energy equation usually only takes less than 5 iterations.[e] Thus, the computational cost for the linear algebra subroutine for the electron continuum model is much smaller than the ion kinetic module.

V. Mode Transition Results

Table 2 shows the four test cases performed using the 2D hybrid-DK simulation. The notation G and L denote the global and local oscillation modes for $B = 120$ G and $B = 180$ G, respectively. The effect of ion gyromotion on the discharge plasma oscillation is first investigated by turning on and off the Lorentz force.

Table 2. Test cases performed using the 2D hybrid-DK simulation

	$B = 120$ G Global mode	$B = 180$ G Local mode
1D Hybrid-DK	1D-G	1D-L
2D Hybrid-DK (With $\mathbf{v} \times \mathbf{B}$)	G-yes	L-yes

The 1D hybrid-DK simulations developed in Ref. 24 are the baseline cases. It is thus expected that the 2D hybrid-DK simulations will capture the azimuthal transport or oscillations while observing the same mode transition phenomena as the 1D hybrid simulations.

A. 1D Hybrid-DK Simulation

The 1D hybrid-DK simulation results serve as the baseline for the 2D hybrid-DK simulations. The main purpose of the 2D simulations is to capture the mode transition and investigate azimuthally rotating structures.

Figure 6 shows the mode transition results obtained from the 1D hybrid-DK simulation. It can be seen that the discharge current oscillations are strong for $B = 120$ G and stabilized for $B = 180$ G. The mean

[d]Physically speaking, Joule heating may not be applicable in the azimuthal direction due to its large Knudsen number.
[e]Note that numerical convergence of the elliptic PDE for the plasma potential was very severe for the 2D drift-diffusion approximation both in the axial and azimuthal directions.

discharge current is about 20 % larger than experimental data of the SPT-100 thruster, which is due to the anomalous electron mobility terms used in the simulations. Although the time-averaged numerical results differ from the experiments, the mode transition is well captured by the 1D hybrid-DK simulation.

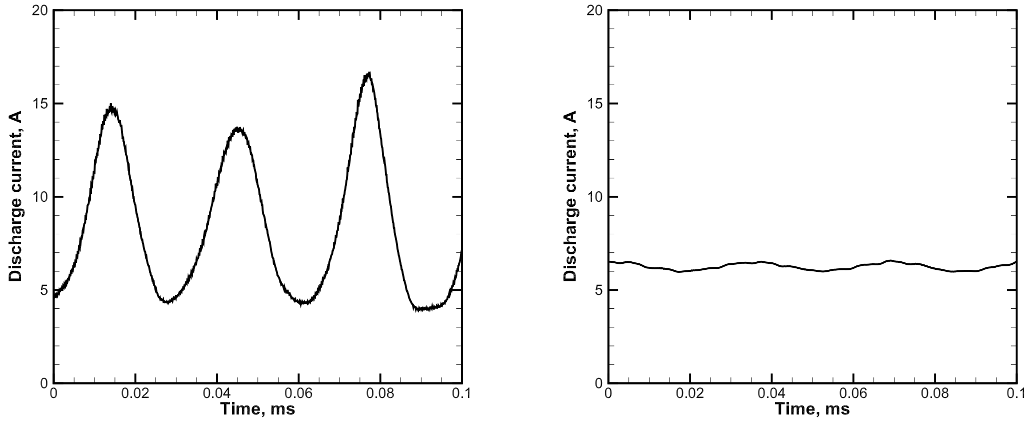

(a) Case 1D-G, $B = 120$ G

(b) Case 1D-L, $B = 180$ G

Figure 6. Discharge oscillations obtained from the 1D hybrid-DK simulation. Note that y-axis is from $I_d = 0-20$ A.

B. Results Including Ion Magnetization

Figure 7 shows the discharge current oscillations obtained from the 2D hybrid-DK simulation with ion magnetization included. The differences between the present 2D simulation and the previous 1D simulation are ion 2D transport in physical space and velocity space, including the electric field and Lorentz force, the 2D electric field structure, and the azimuthal heat flux in the electron energy equation.

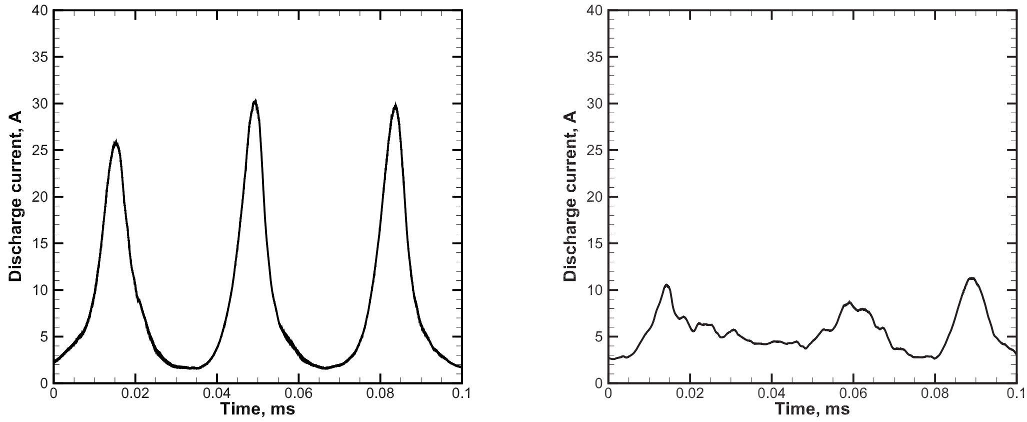

(a) Case G-yes, $B = 120$ G

(b) Case L-yes, $B = 180$ G

Figure 7. Discharge oscillations obtained from the 2D hybrid-DK simulation with Lorentz force. Note that y-axis is from $I_d = 0 - 40$ A.

In comparison to the 1D hybrid-DK simulation, the discharge oscillations are slightly larger in the 2D hybrid-DK simulation. For instance, the maximum and minimum currents obtained from the 1D cases are

17 A and 4 A, whereas those from the 2D cases are 30A and 2 A, respectively, at $B = 120$ G. A similar trend is observed at $B = 180$ G. However, the results for $B = 180$ G exhibit stabilization of the discharge current compared to the results for $B = 120$ G while some high-order oscillatory modes are present. Thus, it can be concluded that mode transition of discharge oscillations are captured with the 2D hybrid-DK simulation. The plasma oscillations are discussed in more detail in the next section.

VI. Plasma Oscillations

The low-frequency plasma oscillations are investigated in this section for the global and local oscillation modes at $B = 120$ G and $B = 180$ G. The results shown are the 2D hybrid-DK simulations with ion magnetization on, *i.e.* Cases G-yes and L-yes listed in Table 2.

A. Global Oscillation Mode

Discharge current oscillations are due to the ionization oscillations in the Hall thruster discharge channel. Figures 8 and 9 show the ion number density and ground-state neutral atom density at two different time steps. $t = t_{id,max}$ corresponds to the time at which the discharge current is at maximum while $t = t_{id,min}$ is when the discharge current is at minimum. For instance, $t_{id,min} = 0.03$ ms and $t_{id,max} = 0.047$ ms in Fig. 7(a).

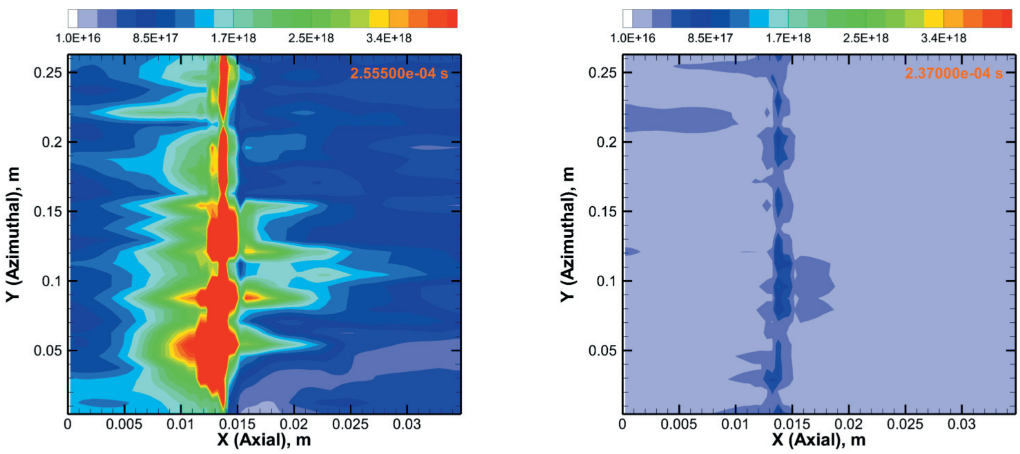

(a) $t = t_{id,max}$

(b) $t = t_{id,min}$

Figure 8. Ion number density in global oscillation mode: $B = 120$ G. The units are in m^{-3}.

An increase in the ion density is associated with depletion of neutral atoms when the discharge current is at maximum. As the ions are accelerated out of the channel and also diffuse to the anode walls, the ion density inside the channel decreases. The ion density is almost an order of magnitude smaller at $t = t_{id,min}$ compared to that at $t = t_{id,max}$. It can be seen that the neutral atoms fill up the ionization region at $t = t_{id,min}$.

The azimuthal electric fields shown in Fig. 10 are large-scale phenomena, $m \approx 7$, where m is the spoke order. However, such azimuthal modes are not important in a global ionization mode because the low-frequency plasma oscillations in the axial direction due to heavy species, *i.e.* ion and neutral atoms, dominate in the discharge channel.

B. Local Oscillation Mode

The transition between the global mode and local mode in Ref. 5 was discussed extensively using a so-called spoke surface plot. The spoke surfaces are calculated from the light intensity obtained from images using a FastCam video, pixelating the images and converting them into a contour map with horizontal axis being time and vertical axis being the azimuthal locations.

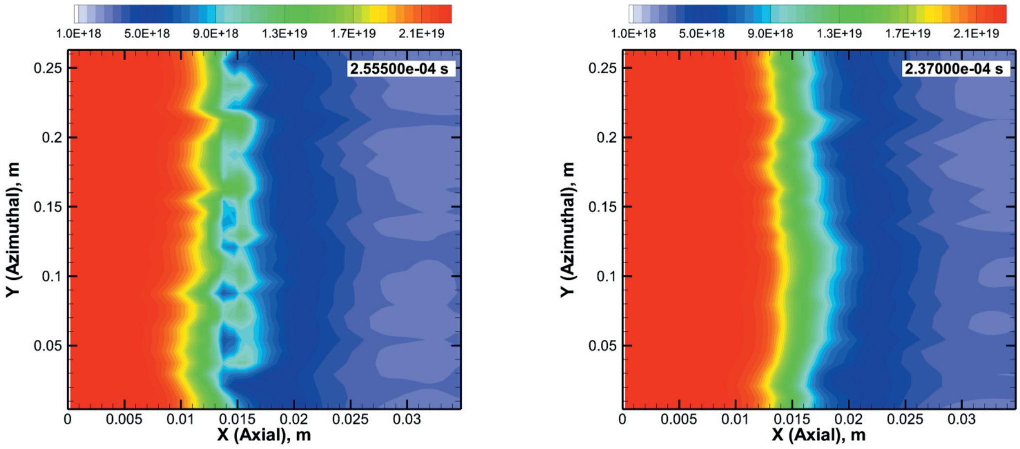

(a) $t = t_{id,max}$ (b) $t = t_{id,min}$

Figure 9. Ground-state neutral atom density in global oscillation mode: $B = 120$ G. The units are in m^{-3}.

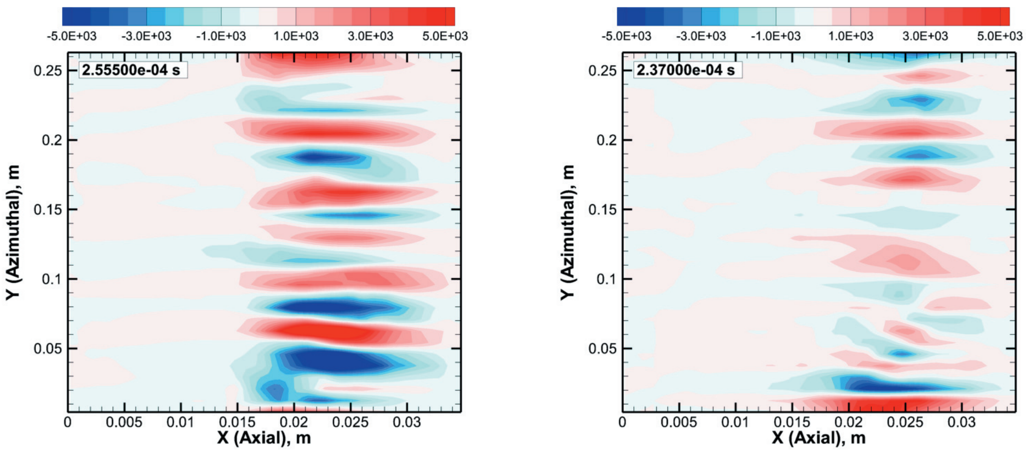

(a) $t = t_{id,max}$ (b) $t = t_{id,min}$

Figure 10. Azimuthal electric field in global oscillation mode: $B = 120$ G. The units are in V/m.

Here, the time evolution of axially-integrated ion density profiles obtained from the 2D hybrid-DK simulation is shown in Fig. 11. Although this may not be exactly the same as the experimental data, it can be assumed that the ion density fluctuations are correlated to the light intensity, which is discussed in Ref. 24.

It can be seen from Fig. 11 that the axial ionization oscillations are reduced in local mode compared to global mode, which agrees with the stabilization of discharge current oscillations. However, it is difficult to observe a clear characteristic azimuthal oscillation wave. One further assumption that can be made is that the axial oscillation needs to be significantly suppressed in order to observe the azimuthal spokes. This also agrees with Sekerak's observations that it was difficult to observe the rotating structures in the presence of a strong global oscillation.[5] It can be considered that a strong axial oscillation mode can hinder the azimuthal oscillations.

Therefore, the relative intensity of the ion number densities can be investigated assuming that axial

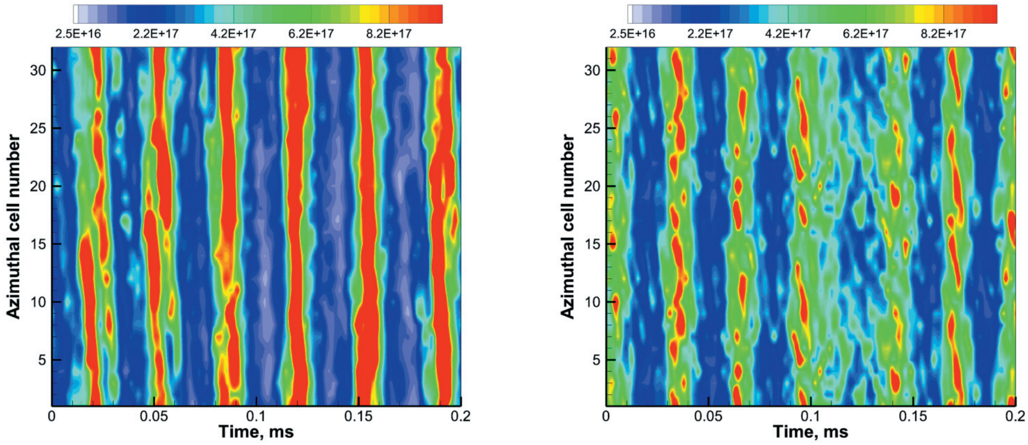

(a) $B = 120$ G

(b) $B = 180$ G

Figure 11. Surface plot of the axially-integrated ion number density.

global oscillations are stabilized. The relative intensity of a quantity Q can be defined as

$$\Sigma_Q(J,t) = 2\frac{Q(J,t) - Q_{mid}(t)}{Q_{max(t)} - Q_{min}(t)}, \tag{20}$$

where Q_{max}, Q_{min}, and Q_{mid} are the maximum, minimum, and average of the maximum and minimum of the signal Q, and Q is a function of time t and the azimuthal cell number J. This essentially transforms Σ_Q between -1 to 1, which is similar to the method used to obtain the normalized spoke surface plots in Refs. 27 and 5.

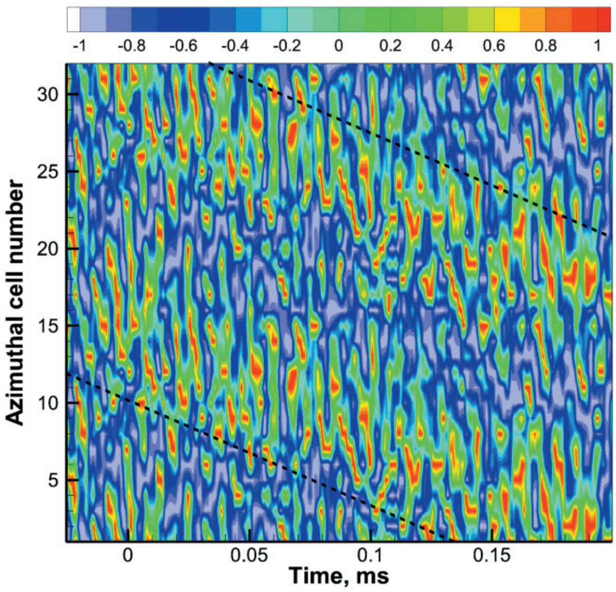

Figure 12. Normalized surface plot of local mode obtained from the 2D hybrid-DK simulation. A line is manually drawn that indicates an azimuthal structure.

Figure 12 shows the relative intensity of the axially-integrated ion number density calculated from Eq.

(20). A dashed line is manually drawn indicating an azimuthally rotating structure. The speed of the rotating structure calculated from the slope is approximately 650−800 m/s, which is smaller than that of the azimuthal spokes observed in Sekerak's experiments, *i.e.* 1500 − 2200 m/s. This disagreement is likely due to the geometric difference as the SPT-100 thruster is assumed in the simulation whereas Sekerak's experiment used the H6 thruster.

It can be noted that the direction of the rotation is in the $-E \times B$ drift since $+y$ direction is the direction of the $E \times B$ drift. Experiments on a cylindrical HET by Parker[1] and on the H6 by Sekerak[5] both showed that the azimuthal spokes propagate in the $+E \times B$ direction. However, it may be worth mentioning that there are observations of the rotating structures in the $-E \times B$ direction in another $E \times B$ device.[28]

The rotating spokes can be explained by gradient-drift waves, which occur when spatial gradients exist in plasma properties. The simplest gradient drift wave is the interaction between a density gradient, ∇n, and the magnetic field, B. Since a drift wave will be generated in the $\nabla n \times B$ direction, any gradient based drift wave will be in the direction of $E \times B$ if $\nabla n \parallel E_x$. Note that Frias *et al.*[29] showed that the gradient drift instability can occur when the axial electric field is negative for $\nabla(n/B) < 0$. Here in the simulations, it was found that the axial electric field is negative locally in the region where the ion density at maximum and the region of the maximum ion density is inside the channel, *e.g.* $x = 0.015$ m. It has been observed from experiments, for instance, in internal measurements of the H6 by Reid,[30] that the maximum ion density peak is still inside the channel but much closer to the channel exit. Therefore, it is likely that the direction of the density gradient is the cause of the azimuthal spokes rotating in the opposite direction in the hybrid-DK simulation.

VII. Discussion

The results of the test cases are shown in Table 3. It can be seen that the effect of ion Lorentz force on the discharge plasma is not negligible. Although the discharge oscillations are not completely stable, they become much more stabilized in local mode at $B = 180$ G in comparison to $B = 120$ G.

Table 3. Results of the 2D hybrid-DK simulation

	$B = 120$ G Global mode	$B = 180$ G Local mode
1D Hybrid-DK	Oscillatory	Very Stable
2D Hybrid-DK (With $\mathbf{v} \times \mathbf{B}$)	Oscillatory	Stable

Global oscillation mode and stabilization of the global oscillations are both obtained by the hybrid-DK simulation. The low-frequency azimuthally rotating spokes are captured by taking the relative intensity of the axially-integrated ion number density. It is assumed that global modes are completely stabilized. The propagation of the azimuthal structure is in the $-E \times B$ direction, but this is attributed to the density gradient in the simulations being opposite from experimental observations.

One improvement from the 2D hybrid-PIC simulation by Lam *et al.* is that the simulation does not become unstable due to the numerical instability issue that was reported in Ref. 21. This is due to the use of a simplified electron continuum model, which simplifies the azimuthal transport. Derivation of the present electron model suggests that a 2D model in the azimuthal direction is numerically difficult as the matrix of the constructed elliptic PDE becomes ill-conditioned, which means that either a different numerical method must be used, such as an integration method, or the physical model must be changed.

Although some low-frequency azimuthally rotating structures are captured by the 2D hybrid-DK simulation, there are still remaining questions about rotating spokes. Boeuf[31] showed low-frequency rotating spokes in a magnetron discharge using a 2D full-PIC simulation. It was suggested that the rotating spoke is a double layer, *i.e.* sheath, in the azimuthal direction. A strong charge separation occurs at the edge of the spokes. In addition, it was observed that a small region near the inner wall (the cathode in their simulations) carries a large amount of azimuthal electron current where the spoke is absent.

Acknowledgement

The authors acknowledge the support for this work provided by the U.S. Department of Energy Office of Science, Fusion Energy Sciences Program, Grant DESC0001939, and the Air Force Research Laboratory through the Michigan/Air Force Center of Excellence in Electric Propulsion (MACEEP) grant number F9550-09-1-0695.

References

[1]Parker, J. B., Raitses, Y., and Fisch, N. J., "Transition in electron transport in a cylindrical Hall thruster," *Applied Physics Letters*, Vol. 97, No. 9, 2010, pp. –. doi:10.1063/1.3486164.

[2]Ellison, C. L., Raitses, Y., and Fisch, N. J., "Cross-field electron transport induced by a rotating spoke in a cylindrical Hall thruster," *Physics of Plasmas*, Vol. 19, 2012, pp. 013503.

[3]Lobbia, R. B., *A Time-resolved Investigation of Hall Thruster Breathing Mode*, Ph.D. thesis, University of Michigan, 2010.

[4]McDonald, M., Bellant, C., Pierre, B. S., and Gallimore, A. D., "Measurement of Cross-Field Electron Current in a Hall Thruster Due to Rotating Spoke Instabilities," AIAA 2011-5810, San Diego, CA, August 2011.

[5]Sekerak, M. J., *Plasma Oscillations and Operational Modes in Hall Effect Thrusters*, Ph.D. thesis, University of Michigan, 2014.

[6]Fife, J. M., *Hybrid-PIC Modeling and Electrostatic Probe Survey of Hall Thrusters*, Ph.D. thesis, MIT, 1998.

[7]Parra, F. I., Ahedo, E., Fife, J. M., and Martínez-Sánchez, M., "A two-dimensional hybrid model of the Hall thruster discharge," *Journal of Applied Physics*, Vol. 100, No. 2, 2006, pp. –. doi:10.1063/1.2219165.

[8]Cheng, S., *Modeling of Hall thruster lifetime and erosion mechanisms*, Ph.D. thesis, MIT, 2007.

[9]Hofer, R. R., Katz, I., Mikellides, I. G., Goebel, D. M., Jameson, K. K., Sullivan, R. M., and Johnson, L. K., "Efficacy of Electron Mobility Models in Hybrid-PIC Hall Thruster Simulations," AIAA 2008-4924, Hartford, CT, July 2008.

[10]Koo, J. W. and Boyd, I. D., "Modeling of anomalous electron mobility in Hall thrusters," *Physics of Plasmas*, Vol. 13, No. 3, 2006. doi:10.1063/1.2172191.

[11]Boeuf, J. P. and Garrigues, L., "Low Frequency Oscillations in a Stationary Plasma Thruster," *Journal of Applied Physics*, Vol. 84, No. 7, 1998, pp. 3541–3554. doi:10.1063/1.368529.

[12]Hagelaar, G. J. M., Bareilles, J., Garrigues, L., and Boeuf, J. P., "Two-dimensional model of a stationary plasma thruster," *Journal of Applied Physics*, Vol. 91, No. 9, May 2002, pp. 5592–5598. doi:10.1063/1.1465125.

[13]Keidar, M., Boyd, I. D., and Beilis, I. I., "Plasma flow and plasma-wall transition in Hall thruster channel," *Physics of Plasmas*, Vol. 8, No. 12, December 2001, pp. 5315–5322.

[14]Mikellides, I. G. and Katz, I., "Numerical simulations of Hall-effect plasma accelerators on a magnetic-field-aligned mesh," *Phys. Rev. E*, Vol. 86, Oct 2012, pp. 046703. doi:10.1103/PhysRevE.86.046703.

[15]Geng, J., Brieda, L., Rose, L., and Keidar, M., "On applicability of the thermalized potential solver in simulations of the plasma flow in Hall thrusters," *Journal of Applied Physics*, Vol. 114, No. 10, 2013, pp. –. doi:10.1063/1.4821018.

[16]Hirakawa, M. and Arakawa, Y., "Numerical simulation of plasma particle behavior in a Hall thruster," AIAA Paper 96-3195, Lake Buena Vista, FL, July 1996.

[17]Szabo, J. J., *Fully Kinetic Numerical Modeling of a Plasma Thruster*, Ph.D. thesis, MIT, 2001.

[18]Cho, S., Komurasaki, K., and Arakawa, Y., "Kinetic particle simulation of discharge and wall erosion of a Hall thruster," *Physics of Plasmas (1994-present)*, Vol. 20, No. 6, 2013, pp. –. doi:10.1063/1.4810798.

[19]Adam, J. D., Heron, A., and Laval, G., "Study of stationary plasma thrusters using two-dimensional fully kinetic simulation," *Physics of Plasmas*, Vol. 11, No. 1, January 2004, pp. 295 –305.

[20]Coche, P. and Garrigues, L., "A two-dimensional (azimuthal-axial) particle-in-cell model of a Hall thruster," *Physics of Plasmas (1994-present)*, Vol. 21, No. 2, 2014, pp. –. doi:10.1063/1.4864625.

[21]Lam, C. M., Fernandez, E., and Cappelli, M. A., "A 2-D Hybrid Hall Thruster Simulation That Resolves the E B A 2-D Hybrid Hall Thruster Simulation That Resolves the $\mathbf{E} \times \mathbf{B}$ Electron Drift Direction," *IEEE Transactions on Plasma Science*, Vol. 43, No. 1, 2015, pp. 86–84.

[22]Boeuf, J.-P., "Rotating structures in low temperature magnetized plasmas - Insight from particle simulations," *Frontiers in Physics*, Vol. 2, No. 74, 2014. doi:10.3389/fphy.2014.00074.

[23]Tremolizzo, E., Meier, H., and Estublier, D., "In-flight Disturbance Torque Evaluation of the SMART-1 Plasma Thruster," *Proceedings of the 18th International Symposium on Space Flight Dynamics (ESA SP-548)*, October 2004, pp. 303–306.

[24]Hara, K., Sekerak, M. J., Boyd, I. D., and Gallimore, A. D., "Mode transition of a Hall thruster discharge plasma," *Journal of Applied Physics*, Vol. 115, No. 20, 2014. doi:10.1063/1.4879896.

[25]Smith, A. W. and Cappelli, M. A., "Time and space-correlated plasma potential measurements in the near field of a coaxial Hall plasma discharge," *Physics of Plasmas (1994-present)*, Vol. 16, No. 7, 2009, pp. –. doi:10.1063/1.3155097.

[26]Siddiqui, M. U., Kim, J. F., Jackson, C. D., and Hershkowitz, N., "Presheath and boundary effects on helicon discharge equilibria," *Plasma Sources Science and Technology*, Vol. 24, 2015, pp. 015022.

[27]McDonald, M., *Electron Transport in Hall Thrusters*, Ph.D. thesis, University of Michigan, 2012.

[28]Ito, T. and Cappelli, M., "High Speed Images of Drift Waves and Turbulence in Magnetized Microplasmas," *Plasma Science, IEEE Transactions on*, Vol. 36, No. 4, Aug 2008, pp. 1228–1229. doi:10.1109/TPS.2008.927347.

[29]Frias, W., Smolyakov, A. I., Kaganovich, I. D., and Raitses, Y., "Long wavelength gradient drift instability in Hall plasma devices. II. Applications," *Physics of Plasmas (1994-present)*, Vol. 20, No. 5, 2013, pp. –. doi:10.1063/1.4804281.

[30]Reid, B. M., *The Influence of Neutral Flow Ratein the Operation of Hall Thrusters*, Ph.D. thesis, University of Michigan, 2009.

[31]Boeuf, J. P. and Bhaskar, C., "Rotating Instability in Low-Temperature Magnetized Plasmas," *Phys. Rev. Lett.*, Vol. 111, No. 15, October 2013. doi:10.1103/PhysRevLett.111.155005.